Distribution of Dune Landform on Mars

Li Chao and Dong Zhibao*

Planetary Aeolian Research Institute, Shaanxi Normal University, Xi'an, China

Dune landforms are widely distributed on Mars and contain abundant information about the Martian atmosphere and sedimentary environment. At present, the understanding of Martian dunes and their environmental significance still needs to be further excavated. Sand dunes were investigated on a global scale using high-resolution remote sensing imagery covering Mars, supported by GIS technology. The object of this paper is to obtain dune landform information and analyze its distribution characteristics and patterns. The results indicated that the Martian dunefields are scattered, generally small in scale and spatially distinct. They are mainly concentrated in high-latitude and polar regions, and show latitude zonality. Similar to Earth, Martian dunes are mainly located in low-lying geomorphic units that are conducive to the accumulation of sand. We propose that the limited sand supply is an important feature of the Martian dune development conditions. The scattered distribution of dunefields reflects the lack of loose sediments on Mars as a whole, which provides an important clue to understanding the Martian environment and evolutionary history.

Keywords: Martian geomorphology, aeolian landform, dune geomorphology, distribution pattern, Mars

INTRODUCTION

The exploration of extraterrestrial planets provides new opportunities for the development of earth science. Research on the environment and evolution of extraterrestrial planets based on exploration data is an active field of earth science (Greeley, 2013), and traditional planetary science dominated by astronomy is gradually becoming dominated by earth science. Mars is the current focus of extraterrestrial planetary exploration. Since the successful launch of Mars probes in the 1960s, there have been three space exploration peaks (Zhibao and Ping, 2019). In 2021, China's Tianwen-1 successfully joined the third peak, indicating that Mars research will become an important frontier exploration field in China. The existing detection results have given us an overall understanding of the Martian atmosphere, geology, and geomorphology (Ouyang and Yongliao, 2015). As one of the most active areas of Mars research, geomorphology reflects the current environment and surface processes of Mars, contains critical information about the evolutionary history of Mars, and provides a key reference for the development of Mars exploration plans (Greeley, 2013). Dunefields, craters, volcanoes, and river channels are the earliest recognized types of Martian landforms, and the aeolian landform process is currently the most one on Mars (Bishop, 2018). Since the Mariner 9 probe provided images of Martian aeolian landforms from 1972 to 1973, the study of aeolian landforms has continued, and some preliminary understanding has been achieved about the types, geomorphological features, and evolutionary environment of dune geomorphology on Mars (Tsoar et al., 1979; Ward et al., 1985; Lancaster and Greeley, 1990; Hargitai and Kereszturi, 2015). Furthermore, speculations have been made in some in-depth comprehensive studies on individual regions that have provided valuable clues for understanding the environment and

evolution of Mars (Bridges et al., 2017; Bridges and Ehlmann, 2018; Boazman et al., 2021; Emran et al., 2021). It is worth noting that Mars Global Digital Dune Database (MGD3) has been gradually established and improved (Hayward et al., 2014; Gullikson et al., 2018; Fenton et al., 2019), providing important basic data for exploring the global sand dune distribution and sand transport paths.

Surface processes such as weathering, erosion, and deposition are the most puzzling in Mars' geological history (Carr and Head, 2010; Changela et al., 2021). Because many landforms associated with them do not match their natural environment. In terms of aeolian landform, the modern Martian surface is cold and dry, which is not conducive to the weathering of rocks and the migration of loose sediment. However, the wide distribution of dune landform shows that there must be some mechanism to form and gather these sand particles. This sparked interest and thought on a range of issues. For example, why did Mars, known as the "desert planet", not have a continuous sand sea? Why do dunes appear there? Where does aeolian sand come from? To answer these questions, we need to get rid of the constraints of existing knowledge and experience, and dig deeper into the geomorphological significance of the distribution of sand dunes.

For half a century, people have accumulated a large number of high-resolution remote sensing images covering the entire planet of Mars (Beyer, 2015). Using this information, we have compiled the *Martian Aeolian Landform Map* (Zhibao et al., 2020). By further extracting information from the *Martian Aeolian Landform Map*, we obtained a comprehensive understanding of the geomorphological characteristics of Martian aeolian landforms. This article attempts to analyze the distribution characteristics of the Martian dune geomorphology, explore the aeolian geomorphology contained in the distribution patterns and the significance of the environmental characteristics and evolution of Mars. This preliminary study will provide reference for future Mars exploration and research.

RESEARCH DATA AND METHODS

The identification of dune landforms mainly used the background camera image (CTX RDR) obtained by the Mars Reconnaissance Orbiter (MRO) (resolution 6 m/pixel) (Zurek and Smrekar, 2007) and the thermal radiation imaging system (THEMIS Day IR) (resolution 100 m/pixel) acquired by the Mars Odyssey Mission (Albee et al., 1998). Small dunes were identified using the high-resolution imaging science laboratory images (HiRISE RDR) (resolution: 0.3 m/pixel) obtained by the Mars Reconnaissance Orbiter (McEwen et al., 2007). The altitude measurement and topographic display used the Mars Orbital Laser Altimeter data (MOLA DEM) (resolution: 463 m/pixel) obtained by the Mars Global Surveyor (Smith et al., 2001).

Based on the distribution range of dunefields provided by the Mars Global Digital Dune Database (Hayward et al., 2014), the spatial vectorization tool of the geographic information system software ArcGIS 10.2, and the method of visual interpretation, the outer boundaries of dunefields were re-identified and confirmed using the CTX RDR satellite images. The THEMIS Day IR satellite imagery was used to traverse Mars and supplement the missing dunefields in the database.

Relative to the Earth, a prominent feature of the distribution of dune geomorphology on Mars is that large continuous sand seas with an area of more than 5000 km^2 are rare and are mainly distributed in the north polar region. Even in the same dunefield, the dunes are mostly scattered and discontinuous, so it is necessary to distinguish the differences in the coverage of different dunefields. According to the proportion of the area covered by dunes in the area of a dunefield, the dunefields were divided into five coverage levels: < 10%, 10%–30%, 30%–60%, 60%–80%, and 80%–100%. The coverage rate was calculated using a combination of quantitative and qualitative methods (Ramsdale et al., 2017). The grid was divided at 5°intervals. The ArcGIS 10.2 spatial vectorization tools were used to identify and divide the dunefields with significant differences in dune coverage in each grid cell as the subarea. Three 1 km × 1 km sample regions were designated in the subarea for calculation. The dune coverage area was extracted according to the difference in the albedo between the dunes and interdunal land in the image. Based on the average of the dune coverage of the three sample regions, the dune coverage level of other dunefields in the subareas was determined. The dune coverage distribution range was determined by combining the dunefields with the same coverage level in each grid cell. Due to the small area of dunefields in the low and middle latitude regions and the south polar region, this paper only calculated the dune coverage of the contiguous dunefields in the north polar region.

The ArcGIS 10.2 analysis tools were applied to calculate the dunefield area in the sinusoidal projection, obtain the dunefield area in the 5°interval grid, and statistically analyze the latitude and longitude of the dunefield distribution according to the centroid coordinates of each grid.

Although the total area of dunefields distributed in craters is small, craters are an important geomorphological unit for the distribution of dune geomorphology on Mars. Crater dunes are numerous and widely distributed. Therefore, the distribution patterns of dunefields within craters are analyzed, in which the eccentricity is adopted to characterize the relative location of a dunefield in a crater. By referring to the database data of the *Geological Map of Mars* (Tanaka et al., 2014), the types of geomorphological units were classified, and the dunefield areas and distribution types of geomorphic units were calculated. The centroids of craters and dunefields were obtained using geometric analysis tools. The eccentricity of each dunefield is calculated using:

$$R_s = \frac{D_c}{C_d} \qquad (1)$$

where R_s is the eccentricity of the dunefield, D_c is the distance between the dunefield and the centroid of the crater, and C_d is the radius of the crater. An eccentricity of zero indicates that it is located in the center of the crater, and the greater the value, the farther away the dune is from the center. Accordingly, the spatial location of the dunefield in the crater can be divided into three modes: central (0–0.33), eccentric (0.33–0.66), and side slope (0.66–1) modes (**Figure 1A**). The side slope is the part closest to the inner wall of the crater.
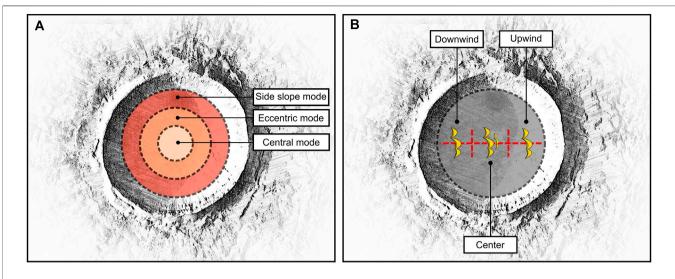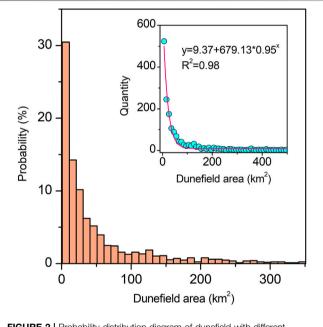
FIGURE 1 | Schematic diagram illustrating the relative locality of dunefield within a crater on Mars. **(A)** Macroscopic distribution patterns of the dunefields. **(B)** spatial location of the dunefields.
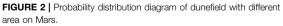
To present the relationship between the distribution of dune geomorphology and the wind direction, the spatial location of a dunefield and the direction of the slip face of transverse dunes (such as Barchan dune and Barchanoid dune) was analyzed. The crater diameter line perpendicular to the ridgeline of the transverse dunes was obtained. By taking one-third of the length as the interval, the location of the dunefield was determined (e.g., upwind, downwind, or in the center of the crater; **Figure 1B**). Among them, the central dunefield was always located in the center of the crater. However, this is only a rough judgment because the relative position cannot be determined for sand dunes with complex shapes.

RESULTS

Probability Distributions of Areas of Dunefields

The statistical results of the areas of dunefields on Mars are as follows: the total area of dunefields is about $98 \times 10^4 \, \text{km}^2$, accounting for only 0.68% of the total surface area of Mars, which is less than the proportion found on Earth (about 1%). The distributions are scattered and extremely uneven (mostly small areas), and true sand seas are rare. Therefore, this article refers to all sand dune distribution areas on Mars as dunefields. The average dunefield area on Mars is approximately $567 \, \text{km}^2$. The largest contiguous dunefield is about $69 \times 10^4 \, \text{km}^2$, accounting for about 70% of the total dunefield area. There are 1720 dunefields larger than $1 \, \text{km}^2$ and 498 dunefields smaller than $10 \, \text{km}^2$, accounting for 29% of the total number of dunefields, yet only 0.24% of the area. There are 1,337 dunefields less than $100 \, \text{km}^2$, accounting for 78% of the total number of dunefields, and 3.32% of the area. Taking statistics at intervals of $10 \, \text{km}^2$, the relationship

FIGURE 2 | Probability distribution diagram of dunefield with different area on Mars.
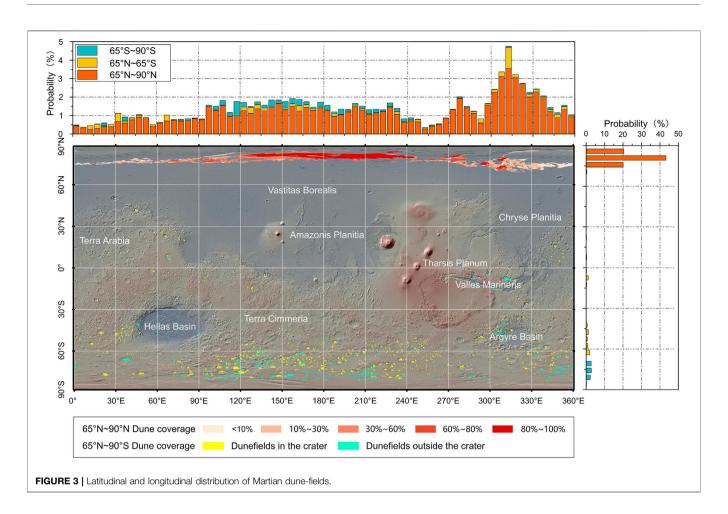
between the area and number of dunefields on Mars can be expressed by an exponential function (**Figure 2**), i.e., the number of dunefields decreases exponentially with the increase in area.

Global Distribution of Dunefields

Figure 3 shows the global distribution characteristics of dunefields on Mars, which can be summarized in three distribution patterns. Firstly, the distributions of

FIGURE 3 | Latitudinal and longitudinal distribution of Martian dune-fields.

dunefields on Mars demonstrate the dichotomy of the northern and southern hemispheres, and are mainly concentrated in the northern hemisphere. The northern and southern hemispheres account for 85.15% and 14.85% of dunefields, respectively, which corresponds to the dichotomy between the landform characteristics of the northern and southern hemispheres on Mars. Secondly, the distribution of Martian dune landform shows latitudinal zonality (**Figure 3**). Although, the current Martian environment is insufficient to form a geographical zonality similar to that of the Earth. According to the regression motion of direct sunlight, Mars is divided into low- and middle-latitude regions as well as high-latitude and polar regions. Dunefields are mainly distributed in the high-latitude and polar regions, which is contrary to the distribution patterns of sand seas on Earth. The distribution of dunefields in the north polar region is the most concentrated, forming a huge but discontinuous ring sand sea around the north polar ice sheet. Among them, about 20% are distributed from 70°N to 75°N; roughly 43% are distributed from 75°N to 80°N; and approximately 20% are distributed from 80°N to 85°N. The south polar region contains the second greatest concentration of dunefields on Mars, most of which are located between 65°S and 80°S. The dunefields are scattered, with an average area of about

$105 \, km^2$, and are mainly found in craters or intermontane depressions. The distribution of dunefields in the low- and middle-latitudes is the sparsest, and most dunefields in these regions are concentrated in the southern hemisphere. The dunefields in the equatorial region are scattered in the northern part of the Valles Marineris, Meridiani Planum, and Terra Cimmeria. The vast northern plains (Vastitas Borealis) have almost no dunefields. Changes in the distribution of dunefields with latitude are also reflected in the types of dunefields. Dunefields in different latitude zones are scattered and extremely uneven, especially in the north polar region (**Figure 4**). In the north polar region, there are 200 dunefields less than $10 \, km^2$ in size, with a probability distribution of 53% and an area percentage of 0.09%; as well as 318 dunefields less than $100 \, km^2$ in size, with a probability distribution of 84% and an area percentage of 0.56%.

Despite the absence of land-sea distribution, the distributions of dunefields on Mars also change with longitude to some extent. Although the difference in meridional distribution is relatively mild, the probability distribution map of the dunefield area on Mars versus longitude shows obvious peaks and troughs (**Figure 3**). The peaks occur around 310–320°E and 270–285°E; gentle peaks appear at roughly 120°E–230°E; and the troughs occur at about 250–260°E, 280–300°E, and 0–30°E.
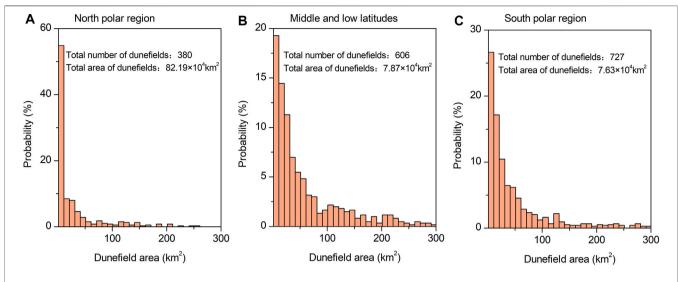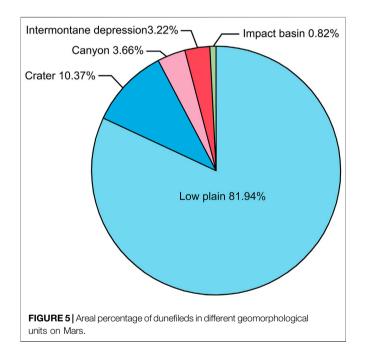
FIGURE 4 | Probability distribution of dune-field area in north polar area, south polar area and mid-low latitude area on Mars. **(A)** North polar region. **(B)** Middle and low latitudes. **(C)** South polar region.

FIGURE 5 | Areal percentage of dunefileds in different geomorphological units on Mars.

Major Geomorphological Units of Dunefield Distribution

Most dunefields on Mars are distributed in five types of geomorphological units (in descending order of dunefield area): low plains, craters, canyons, intermontane depressions, and impact basins (**Figure 5**). The low plains include a concentrated and contiguous distribution area of dunefields, including the northern large plain surrounding the north polar ice sheet. The Olympia Undae is the most typical low plain, with an average altitude of about −5000 m and gentle terrain

undulations. The Promethei Terra, Cimmeria Terra, and Sirenum Terra in the southern hemisphere are the most typical craters, with an average altitude of about 100 m and an altitude difference of about 9000 m. The Chasma Boreale and Valles Marineris in the north polar region are the most typical large canyons, with an altitude of less than −3000 m. The intermontane depressions include undulating and gentle depressions, polar depressions, and cliff bottoms, with an altitude above 1000 m. The western edge of the Argyre Planitia is the most typical impact basin dunefields. The dunefields are distributed in the valley or crater in the basin, and the altitude is less than −1500 m.

Dunefields on Mars are mainly concentrated in low plains. Although the probability of quantity distribution of dunefields here is 18.95%, the proportion of area is 81.94%, which exceeds the total area of other landforms. (**Figure 5**). The ring sand sea surrounding the north polar ice sheet on Mars consists of the largest contiguous dunefield and a high number of small dunefields scattered around it. The probability distributions of dunefields with areas of less than 10 and 100 km^2 are 39.59% and 70.05%, respectively. **Table 1** summarizes the dunefields areas in different geomorphological units on Mars. Among them, the Olympia Undae, with the greatest dune coverage, has a relatively high altitude and is dominated by network dunes. The dune coverage of the Aspledon Undae (the lowest terrain) is generally less than 30%, and is dominated by Barchan dunes (**Figure 3**). Dunefields on Mars are most commonly found in craters. Although the area percentage is only 10.37%, the probability distribution reaches as high as 50.6%. Most crater dunefields are located in the southern hemisphere, and the probability distribution of dunefields with an area less than 100 km^2 is 77.96%. The area percentage of dunefields in intermontane depressions is very small; most of these dunefields are scattered in the high-latitude regions south of 60°S, with a probability distribution of 22.32%. Among them, the probability distribution of dunefields with an area of less than 100 km^2 is 81.51%. The probability

TABLE 1 | Statistics of geomorphological units with dunefields on Mars (unit: km^2).

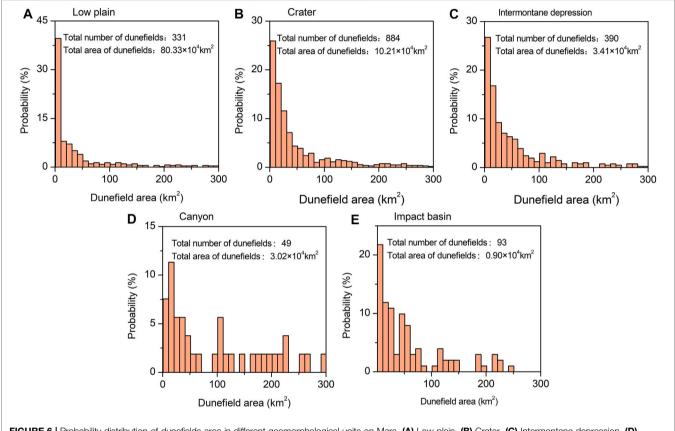| Geomorphological units	Minimum	Maximum	Median	Mean	Variable coefficient
Low plain	1.02	690,940.96	6.75	2,426.88	15.70
Crater	1.02	4683.61	29.64	115.45	2.42
Intermontane depression	1.03	3985.32	28.93	87.49	3.04
Canyon	1.25	8079.11	123.24	616.12	2.40
Impact basin	1.41	937.04	44.96	96.32	1.67

FIGURE 6 | Probability distribution of dunefields area in different geomorphological units on Mars. **(A)** Low plain. **(B)** Crater. **(C)** Intermontane depression. **(D)** Canyon. **(E)** Impact basin.
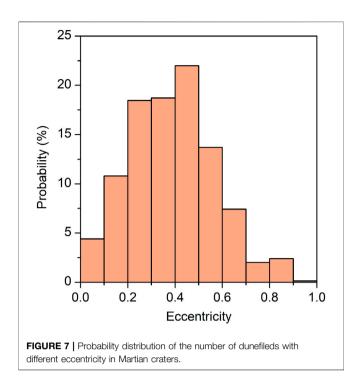
distribution of dunefields in canyon areas is the smallest (only 2.8%), the average area is relatively large (616.12 km^2), and the probability distribution of dunefields with an area less than 100 km^2 is 39.62%. The scale of the Mars impact basin is huge, but dunefields are extremely rare. The area percentage is only 0.82%, the probability distribution is 5.32%, and 73.27% of the dunefields area is less than 100 km^2 (**Figure 6**).

Distribution Patterns of Dunefields in Craters

The majority of crater dunes are concentrated in the highland south of 30°S. There are very few crater dunes in the middle-and low-latitude and north polar regions, demonstrating obvious

TABLE 2 | Latitude distribution of dunefields in Martian craters.

Latitude range	Count	Area (km^2)	Area ratio (%)
65°N~90°N	51	0.32×10^4	3.07
30°S~65°S	392	4.25×10^4	40.58
65°S~90°S	391	4.83×10^4	46.09

characteristics of variation with latitude (**Table 2**). The sand seas that have developed in basins on Earth are usually located in the sediment concentration center in the center of the basin. While the dunefields in Martian craters are similar to the dunefields in Earth basins, they do not always develop in the center of the crater. This paper reveals this characteristic of

FIGURE 7 | Probability distribution of the number of dunefileds with different eccentricity in Martian craters.

Martian crater dunefields by analyzing their eccentricity. The statistical results of the eccentricity show that the average eccentricity of the crater dunefields on Mars is 0.39, and the standard deviation is about 0.18. The greatest proportion of eccentricity was found between 0.4 and 0.5, accounting for about 22%. The area percentage of dunefields with eccentricity of less than 0.5 is about 74.24% (**Figure 7**). The area percentage of eccentric mode dunefields is the highest, followed by the central mode, while that of the side slope mode is the least. According to the relationship between the location of dunefields in craters and the wind direction, the dunefields can be categorized as belonging to the middle type, upwind type, and downwind type, with area percentages of 65.96%, 9.61%, and 15.88%, respectively. For the side slope mode and eccentric mode dunefields, dunefields in the middle location are the most common, while dunefields in the upwind location are the least common (**Table 3**).

Through investigating and analyzing the landform patterns of 796 crater dunefields on Mars, it was found that there were four main macroscopic distribution patterns of dunefields within craters: patchy, planar, circular, and concentric (**Figure 8**) (**Table 4**). Among them, patchy dunefields are the most common, characterized by single or multiple ovals or arc strips (**Figure 8A**) with mostly middle and central mode distributions. The patchy dunefields are dominated by crescentic dune chains, and there are a small number of crescentic, transverse, diagonal, nail, and star dunes. Planar dunefields are characterized by flat sand flakes, mostly in a two-dimensional plane. There are narrow ridges at the edges of the dunefields (**Figure 8B**), reflecting the limited supply of sand sources and the inactive aeolian environment. Planar dunefields are mainly located south of 60°S, and are concentrated in the Promethei Terra and Aonia Terra between 60–120°E and 210–260°E. Patchy and planar dunefields are different in terms of the degree of surface undulation. The former has extreme surface undulations, while the latter has gentle or no topographic undulations. Circular dunefields mostly consist of crescentic dune chains around the central mountain body of the crater, with a small number of sand flakes and dome dunes at the edges (**Figure 8C**). The distribution pattern of circular dunefields is closely related to the topography. The airflow entering the crater is blocked by the central mountain and forms a detour, which causes the aeolian deposits around the mountain to develop a unique circular shape. A concentric dunefield is also known as a bull's-eye dunefield. A typical feature of these dunefields is that they consist of multiple layers of circular dunefield nested in concentric circles. Bull's-eye dunefields are often located in the middle of or adjacent to the crater wall. These dunes have a crescentic or grid shape (**Figure 8D**). Due to the lack of understanding of the local circulation systems of craters, the formation process of concentric dunefields is still unclear. Nevertheless, it is certain that the topography plays a decisive role in controlling the evolution of the dune morphology.

DISCUSSION

Distribution patterns of dunefields on Mars are similar to those of sand seas on Earth, but what is more worthy of attention is its difference. The similarity predominantly lies in the geomorphological units developed by dune landforms. Most of

TABLE 3 | Probability distribution of area and number of dunefields in craters on Mars with different distribution mode.

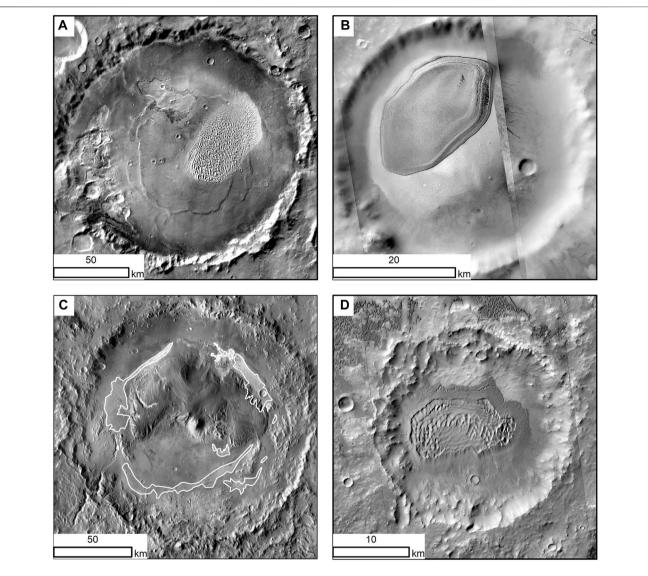| Spatial location	Side slope mode		Eccentric mode		Central mode	
	Area scale (%)	Quantity scale (%)	Area scale (%)	Quantity scale (%)	Area scale (%)	Quantity scale (%)
Upwind	1.26	0.57	8.35	5.38		
Downwind	3.96	1.34	11.92	11.27		
Center	5.60	4.92	19.28	32.18	41.08	38.24
Not determinable	0.53	0.45	8.02	5.66		
Total	11.35	7.27	47.57	54.48	41.08	38.24

FIGURE 8 | Distribution patterns of dunefields within craters on Mars [**(A)** patchy; **(B)** planar; **(C)** circular; **(D)** concentric].

TABLE 4 | Probability distribution of area and number of dunefields in craters on Mars with different macroscopic distribution patterns.

Distribution pattern	Percentage (%)	Area ratio (%)	Average area (km^2)	Percentage to the area of crater bottom (%)
Patchy	88.07	83.23	80	8
Planar	7.79	6.93	194	20
Circular	1.26	7.55	408	4
Concentric	2.89	2.29	352	30

Earth's sand seas are found in geomorphological units that are conducive to the collection of sediment (such as basins, alluvial plains, and river valleys). The geomorphological units of dunefields on Mars (such as low plains, craters, large canyons, intermontane depressions, and impact basins) are also places where sediment is relatively concentrated. For example, Martian arctic dunes are mainly located in the low plains and have a sharp elevation difference with the polar ice caps. The low-lying and open topographical conditions are conducive to the collection and migration of sand sources. On the one hand, the prevailing

westerly winds from the mid-latitudes are reduced in wind speed after encountering large topographical obstacles, creating a low-wind-energy environment at the edge of the ice sheet. This provides favorable conditions for aeolian sand deposition. On the other hand, prominent topographic boundaries have strong thermal gradients that may lead to seasonal gravitational wind, which in turn drives aeolian sand activity (Warner and Farmer, 2008; Chojnacki et al., 2019). The difference predominantly lies in the different key environmental elements that control the development of dune landforms. The formation of aeolian landforms requires two basic conditions: abundant loose sediment and arid and windy climate conditions. On Earth, abundant loose sediment formed during the Quaternary period, and wet and dry climates controlled the formation of dune landforms and the extent of sand seas (Thomas and Wiggs, 2008). Sand seas on Earth can therefore be called the climate-controlled type. In contrast, Mars has a long history of a cold and arid environment (Carr and Head, 2010), which highlights the importance of sediment in the development of dune landforms. In fact, other key features of dunefields on Mars, such as the simplicity of type and geomorphological characteristics, have been attributed to the inadequate sediment supply, i.e., "malnourished dunes" (Li et al., 2020). Therefore, Martian dunefields can be called the sediment-controlled type. The abundance of sediment is one of the key factors for understanding the Martian aeolian geomorphology.

Because Earth and Mars each demonstrate one of the two basic conditions for the formation of aeolian landforms, they exhibit overall opposite distribution patterns. The aeolian landforms on Earth are mainly distributed in the low-latitude regions under the control of subtropical high pressure and mid-latitude temperate arid regions. However, aeolian landforms are extremely scarce in the poles and high latitudes. For the most part, dunefields on Mars are distributed at the poles and in high-latitude regions, particularly in the North Pole, and there are very few in the low- and middle-latitude regions. Affected by the distribution of land and sea, the temperate deserts on the Earth are distributed on the inland or the west coast of the continent (South America). Although the dunefields on Mars are distributed differently in longitude, they reflect the formation conditions of loose sediment, and are unaffected by land and sea distribution. Therefore, the zonality of Martian dunefield distribution is fundamentally unlike that of Earth sand sea distribution. The former reflects the latitude differences of loose sediment formation conditions, and the influencing factors are simple. While, the latter corresponds to the geographical zonality, and the influencing factors are complex.

The weathering effect on the Earth has been strong since the Quaternary period. Even in arid regions, fresh debris cone are routinely formed, which provide fresh sediment to the sand sea (Harvey, 2013), such as the huge amount of weathering material in the dry mountains around the Tarim Basin. It is understandable that Mars currently lacks biological weathering and chemical weathering. However, why is its physical weathering so weak despite the fact that its daily temperature fluctuations are much greater than those of Earth? This is largely due to the long-lasting dry environment on Mars. Physical weathering in arid regions on Earth is so strong due

to the intervention of water. Even in the driest regions on the Earth, the existence of water in different forms can greatly accelerate the weathering process through freezing, thawing, and salt weathering (Camuffo, 1995). But, the physical weathering on Mars (especially in the low- and middle-latitude regions) does not involve water. Thus, salt weathering does not occur even though Mars has extensive saline-alkali land. Therefore, the role of water in planetary surface processes is significant. Mars is now a silent planet, and surface processes are extremely slow. Although the aeolian process is the main surface process at present, its intensity is far weaker than that of Earth. Aeolian weathering on Mars is so limited that it cannot form extensive dunefields, let alone the vast seas of sand found on Earth. In this sense, water is not only a clue to potentially finding evidence of life (Domagal-Goldman et al., 2016), but also a key factor in understanding the surface processes on Mars (Soderblomand and Bell, 2008). The distribution characteristics and patterns of dunefields on Mars can provide important inspiration for elucidating the Martian water environment.

Despite the lack of loose sediment on Mars, there are some sedimentary rocks (including ancient hydrosedimentary and aeolian sedimentary rocks) and outcrops rich in carbonates, sulfates, and SiO_2 (Morris Richard et al., 2010; Hayes et al., 2011), indicating that there was once a water-rich environment. Studies have shown that the warm and water-rich environment in the middle to late Noahian (4.1–3.7 Ga) caused the extensive development of dendritic channels. Overflowing rivers in the Western period (3.7–2.9 Ga) produced a large amount of sediment, which either became direct sediment for developing aeolian landforms or formed sedimentary rocks that turned into sediment (through weathering and denudation) for developing aeolian landforms. The Amazonian (since 2.9 Ga) has had a long time span, accounting for almost 60% of the evolutionary history of Mars (Carr and Head, 2010). During the Amazonian, the surface of Mars extreme drought and the surface processes on Mars became dominated by aeolian processes. The Amazonian can therefore be called the desert period to some extent. Nonetheless, despite such a long desert period, dunefields only account for 0.68% of the area of Mars. This is because the lack of water leads to slow surface processes and limited loose sediment. In this sense, the long history of drought is the limiting factor in the formation of dunefields on Mars, in contrast to the effect of drought on Earth. To understand the formation of aeolian landforms and dunefields on Mars, it is also necessary to fully understand the role of flowing water in the formation of loose sediment. Water should be an important target of Mars exploration. Geomorphological characteristics of dunefields on Mars (including their distribution patterns) can provide information about the water environment of Mars. However, the phenomenon of flowing water is not necessarily driven by climatic factors, but may also be a seepage caused by thermal melting (McKenzie and Nimmo, 1999). Hence, the study of dunefields on Mars has far-reaching significance.

Since the Amazonian, the geomorphological processes represented by impacts, tectonics and volcanic activity have been very slow compared with the early period, and the rate of erosion and weathering has been very low. But geomorphological phenomena involving ice and wind are

more pronounced, especially in mid-to-high latitudes (Carr and Head, 2010). The periodic changes of orbital inclination, perihelion and eccentricity determine the amount of solar radiation reaching the surface and affect the stability of ice at various latitudes, thus forming a climate cycle similar to the alternating glacial and interglacial periods on Earth (Laskar et al., 2002). The stability of surface ice is sensitive to changes in the orbital inclination and may be redistributed globally with climate change. This makes the landforms related to freezing show a significant latitudinal distribution feature (Mangold, 2005; Kereszturi et al., 2011; Harrison et al., 2015; Johnsson et al., 2018). Under the dry and cold environment, both the periglacial landforms (including Polygonal feature, Gully and Solifluction lobe) and the dune landforms show the zonal characteristics of middle and high latitude, and have a good spatial consistency with the distribution of global ice (Feldman et al., 2004; Mangold, 2005; Harrison et al., 2015; Johnsson et al., 2018). During the formation of periglacial landforms, loose sediments are disturbed and re-sorted along with the fragmentation of rocks. The rock and soil are subjected to repeated freeze-thaw action, and the silt content increases (Corte, 1963; Williams, 2017). It should be pointed out that there have been almost no environmental conditions on the surface of Mars that can sustain liquid water since the Amazonian (Levy et al., 2009). The "freeze-thaw action" here refers to the effect of water or CO_2 on the surface structure and morphology through the phase change between sublimation and deposition. Therefore, the loose and broken material produced by the freeze-thaw action may also be an important source of sand for dune formation.

In addition, the dark layers exposed in the crater walls and beneath some crater floors are the possible local source of dark intracrater aeolian deposits (Tirsch et al., 2011). The results of spectral analysis show that the aeolian deposits of almost all Martian craters have the same mafic mineralogical composition, which points to an origin of volcanic eruptions. Dark deposits found in the crater walls may indicate a global distribution of volcanic ash deposits in the early Noahian period. After the action of groundwater, meteorite impact and crustal movement in the later period, these dark layers were broken, providing sand source for sand dune formation. Moreover, the dark layers buried in the ground avoid the effects of chemical weathering caused by later running water, and are only exposed and moved by a series of erosions after the wet period (Tirsch et al., 2011). Considering the complexity of the geographical environment of the Martian dune distribution area, it can be inferred that the sources of aeolian sand may be diverse.

CONCLUSION

Based on high-resolution remote sensing image data covering the whole planet of Mars, with the support of geographic information technology, the dune landforms were investigated on a global scale. The area, latitude and longitude range, and located geomorphic unit of Martian sand dunes, and the dune pattern in the craters were analyzed in detail. The main findings are as follows:

(1) Dunefields are scattered and generally small in scale, and the average area is about 567 km^2. The total area of Martian dunefields is about 98×10^4 km^2, accounting for 0.68% of the total surface area. Although the global climate of Mars is extremely arid and has a long history of drought, most of the dunefields are small, and a large continuous sand sea is rare. There are 1,720 dunefields larger than 1 km^2, and about 30% of dunefields are less than 10 km^2.

(2) The distributions of dunefields demonstrate a significant dichotomy between the northern (85.15%) and southern (14.85%) hemispheres. The distributions of dunefields present latitude zonality, and are concentrated in high-latitude and polar regions (the dunefields north of 65°N account for 84.25%, the dunefields south of 65°S account for 7.68%, and the range between 65°N and 65°S accounts for 7.93%).

(3) Most dunes develop in topographic depressions, including Low plains, Craters, Large canyons, Intermontane depressions, and Impact basins, accounting for 81.94%, 10.37%, 3.66%, 3.22%, and 0.82%, respectively.

(4) Despite the relatively small total area of dunefields in craters, craters are a representative of the development environment. The distribution patterns of dunefields in craters include patchy, planar, circular, and concentric forms, but patchy landforms dominate. Based on the relative location of dunefields in craters, they can be divided into eccentric, central, and side slope modes, accounting for 47.57%, 41.08%, and 11.35%, respectively.

The distribution patterns of Martian dunefields show that, unlike on Earth, the limited sand supply is the dominant environmental factor controlling the development of dune landforms. The scattered distribution of dunefields reflects the absence of loose sediments on Mars, providing important clues to the planet's environment and evolutionary history.

DATA AVAILABILITY STATEMENT

The raw data supporting the conclusion of this article will be made available by the authors, without undue reservation.

AUTHOR CONTRIBUTIONS

LC is mainly responsible for data collection, processing, mapping and manuscript writing. DZ is responsible for topic selection, discussion and article polishing.

FUNDING

REFERENCES

Abrevaya, X. C., Anderson, R., Arney, G., Atri, D., Azúa-Bustos, A., Bowman, J. S., et al. (2016). The Astrobiology Primer v2.0. *Astrobiology* 16 (8), 561–653. doi:10.1089/ast.2015.1460

Albee, A. L., Palluconi, F. D., and Arvidson, R. E. (1998). Mars Global Surveyor Mission: Overview and Status. *Science* 279 (5357), 1671–1672. doi:10.1126/science.279.5357.1671

Beyer, R. A. (2015). An Introduction to the Data and Tools of Planetary Geomorphology. *Geomorphology* 240, 137–145. doi:10.1016/j.geomorph.2014.11.022

Bishop, M. A. (2018). "Dark Dunes of Mars," in *Dynamic Mars*. Editors R. J. Soare, S. J. Conway, and S. M. Clifford (Elsevier), 317–360. doi:10.1016/b978-0-12-813018-6.00011-x

Boazman, S. J., Davis, J. M., Grindrod, P. M., Balme, M. R., Vermeesch, P., and Baird, T. (2021). Measuring Ripple and Dune Migration in Coprates Chasma, Valles Marineris: A Source to Sink Aeolian System on Mars? *J. Geophys. Res. Planets* 126 (3), e2020JE006608. doi:10.1029/2020JE006608

Bridges, N. T., and Ehlmann, B. L. (2018). The Mars Science Laboratory (MSL) Bagnold Dunes Campaign, Phase I: Overview and Introduction to the Special Issue. *J. Geophys. Res. Planets* 123 (1), 3–19. doi:10.1002/2017je005401

Bridges, N. T., Sullivan, R., Newman, C. E., Navarro, S., van Beek, J., Ewing, R. C., et al. (2017). Martian Aeolian Activity at the Bagnold Dunes, Gale Crater: The View from the Surface and Orbit. *J. Geophys. Res. Planets* 122 (10), 2077–2110. doi:10.1002/2017je005263

Camuffo, D. (1995). Physical Weathering of Stones. *Sci. Total Environ.* 167 (1), 1–14. doi:10.1016/0048-9697(95)04565-I

Carr, M. H., and Head, J. W. (2010). Geologic History of Mars. *Earth Planet. Sci. Lett.* 294 (3), 185–203. doi:10.1016/j.epsl.2009.06.042

Changela, H. G., Chatzitheodoridis, E., Antunes, A., Beaty, D., Bouw, K., Bridges, J. C., et al. (2021). Mars: New Insights and Unresolved Questions. *Int. J. Astrobiology* 20 (6), 394–426. doi:10.1017/S1473550421000276

Chojnacki, M., Banks, M. E., Fenton, L. K., and Urso, A. C. (2019). Boundary Condition Controls on the High-Sand-Flux Regions of Mars. *Geology* 47 (5), 427–430. doi:10.1130/g45793.1

Corte, A. E. (1963). Particle Sorting by Repeated Freezing and Thawing. *Science* 142 (3591), 499–501. doi:10.1126/science.142.3591.499

Emran, A., Marzen, L. J., King Jr., D. T., Jr, and Chevrier, V. F. (2021). Thermophysical and Compositional Analyses of Dunes at Hargraves Crater, Mars. *Planet. Sci. J.* 2 (6), 218. doi:10.3847/PSJ/ac25ee

Feldman, W. C., Prettyman, T. H., Maurice, S., Plaut, J. J., Bish, D. L., Vaniman, D. T., et al. (2004). Global Distribution of Near-Surface Hydrogen on Mars. *J. Geophys. Res.* 109 (E9), E09006. doi:10.1029/2003JE002160

Fenton, L. K., Gullikson, A. L., Hayward, R. K., Charles, H., and Titus, T. N. (2019). The Mars Global Digital Dune Database (MGD3): Global Patterns of mineral Composition and Bedform Stability. *Icarus* 330, 189–203. doi:10.1016/j.icarus.2019.04.025

Greeley, R. (2013). *Introduction to Planetary Geomorphology*. Cambridge University Press.

Gullikson, A. L., Hayward, R. K., Titus, T. N., Charles, H., Fenton, L. K., Hoover, R. H., et al. (2018). "Mars Global Digital Dune Database (MGD3)—Composition, Stability, and thermal Inertia," in *Open-File Report* (Reston, VA, 1164.

Hargitai, H., and Kereszturi, Á. (2015). *Encyclopedia of Planetary Landforms*. New York: Springer.

Harrison, T. N., Osinski, G. R., Tornabene, L. L., and Jones, E. (2015). Global Documentation of Gullies with the Mars Reconnaissance Orbiter Context Camera and Implications for Their Formation. *Icarus* 252, 236–254. doi:10.1016/j.icarus.2015.01.022

Harvey, A. (2013). "Processes of Sediment Supply to Alluvial Fans and Debris Cones," in *Dating Torrential Processes on Fans and Cones: Methods and Their Application for Hazard and Risk Assessment*. Editors M. Schneuwly-Bollschweiler, M. Stoffel, and F. Rudolf-Miklau (Dordrecht: Springer Netherlands), 15–32. doi:10.1007/978-94-007-4336-6_2

Hayes, A. G., Grotzinger, J. P., Edgar, L. A., Squyres, S. W., Watters, W. A., and Sohl-Dickstein, J. (2011). Reconstruction of Eolian Bed Forms and Paleocurrents from Cross-Bedded Strata at Victoria Crater, Meridiani Planum, Mars. *J. Geophys. Res.* 116 (E7), E00F21. doi:10.1029/2010JE003688

Hayward, R. K., Fenton, L. K., and Titus, T. N. (2014). Mars Global Digital Dune Database (MGD3): Global Dune Distribution and Wind Pattern Observations. *Icarus* 230, 38–46. doi:10.1016/j.icarus.2013.04.011

Johnsson, A., Conway, S. J., Reiss, D., Hauber, E., and Hiesinger, H. (2018). "Slow Periglacial Mass Wasting (Solifluction) on Mars," in *Dynamic Mars*, 239–269. doi:10.1016/b978-0-12-813018-6.00008-x

Kereszturi, A., Möhlmann, D., Berczi, S., Horvath, A., Sik, A., and Szathmary, E. (2011). Possible Role of Brines in the Darkening and Flow-like Features on the Martian Polar Dunes Based on HiRISE Images. *Planet. Space Sci.* 59 (13), 1413–1427. doi:10.1016/j.pss.2011.05.012

Lancaster, N., and Greeley, R. (1990). Sediment Volume in the north Polar Sand Seas of Mars. *J. Geophys. Res.* 95 (B7), 10921. doi:10.1029/JB095iB07p10921

Laskar, J., Levrard, B., and Mustard, J. F. (2002). Orbital Forcing of the Martian Polar Layered Deposits. *Nature* 419 (6905), 375–377. doi:10.1038/nature01066

Levy, J. S., Head, J. W., and Marchant, D. R. (2009). Cold and Dry Processes in the Martian Arctic: Geomorphic Observations at the Phoenix landing Site and Comparisons with Terrestrial Cold Desert Landforms. *Geophys. Res. Lett.* 36 (21), L21203. doi:10.1029/2009GL040634

Li, C., Dong, Z., Lv, P., Zhao, J., Fu, S., Feng, M., et al. (2020). A Morphological Insight into the Martian Dune Geomorphology. *Chin. Sci. Bull.* 65 (01), 80–90. doi:10.1360/tb-2019-0168

Mangold, N. (2005). High Latitude Patterned Grounds on Mars: Classification, Distribution and Climatic Control. *Icarus* 174 (2), 336–359. doi:10.1016/j.icarus.2004.07.030

McEwen, A. S., Eliason, E. M., Bergstrom, J. W., Bridges, N. T., Hansen, C. J., Delamere, W. A., et al. (2007). Mars Reconnaissance Orbiter's High Resolution Imaging Science Experiment (HiRISE). *J. Geophys. Res.* 112 (E5), E05S02. doi:10.1029/2005je002605

McKenzie, D., and Nimmo, F. (1999). The Generation of Martian Floods by the Melting of Ground Ice above Dykes. *Nature* 397 (6716), 231–233. doi:10.1038/16649

Morris, R. V., Ruff, S. W., Gellert, R., Ming, D. W., Arvidson, R. E., Clark, B. C., et al. (2010). Identification of Carbonate-Rich Outcrops on Mars by the Spirit Rover. *Science* 329 (5990), 421–424. doi:10.1126/science.1189667

Ouyang, Z., and Yongliao, Z. (2015). *Introduction to Mars Science*. Shanghai: Shanghai Science and Technology Education Press.

Ramsdale, J. D., Balme, M. R., Conway, S. J., Gallagher, C., van Gasselt, S. A., Hauber, E., et al. (2017). Grid-based Mapping: A Method for Rapidly Determining the Spatial Distributions of Small Features over Very Large Areas. *Planet. Space Sci.* 140, 49–61. doi:10.1016/j.pss.2017.04.002

Smith, D. E., Zuber, M. T., Frey, H. V., Garvin, J. B., Head, J. W., Muhleman, D. O., et al. (2001). Mars Orbiter Laser Altimeter: Experiment Summary after the First Year of Global Mapping of Mars. *J. Geophys. Res.* 106 (E10), 23689–23722. doi:10.1029/2000JE001364

Soderblomand, L. A., and Bell, J. F., III (2008). "Exploration of the Martian Surface: 1992–2007," in *The Mars Surface Composition, Mineralogy and Physical Properties*. Editor J. Bell (Cambridge, UK: Cambridge University Press), 3–19.

Tanaka, K. L., Skinner, J. A., Jr, Dohm, J. M., Irwin, R. P., Kolb, E. J., Fortezzo, C. M., et al. (2014). *Geologic Map of Mars: U.S. Geological Survey Scientific Investigations Map 3292, Scale 1:20,000,000*. pamphlet 43 p. Arizona: U.S. Geological Survey.

Thomas, D. S. G., and Wiggs, G. F. S. (2008). Aeolian System Responses to Global Change: Challenges of Scale, Process and Temporal Integration. *Earth Surf. Process. Landforms* 33 (9), 1396–1418. doi:10.1002/esp.1719

Tirsch, D., Jaumann, R., Pacifici, A., and Poulet, F. (2011). Dark Aeolian Sediments in Martian Craters: Composition and Sources. *J. Geophys. Res.* 116 (E3), E03002. doi:10.1029/2009je003562

Tsoar, H., Greeley, R., and Peterfreund, A. R. (1979). MARS: The North Polar Sand Sea and Related Wind Patterns. *J. Geophys. Res.* 84 (B14), 8167. doi:10.1029/JB084iB14p08167

Ward, A. W., Doyle, K. B., Helm, P. J., Weisman, M. K., and Witbeck, N. E. (1985). Global Map of Eolian Features on Mars. *J. Geophys. Res.* 90 (B2), 2038–2056. doi:10.1029/JB090iB02p02038

Warner, N. H., and Farmer, J. D. (2008). The Origin of Conical mounds at the Mouth of Chasma Boreale. *J. Geophys. Res.* 113 (E11), E11008. doi:10.1029/2007je003028

Williams, P. W. (2017). "Wearing it Down," in *New Zealand Landscape*, 119–184. doi:10.1016/b978-0-12-812493-2.00004-9

Zhibao, D., and Ping, L. (2019). Aeolian Geomorphology in the Era of Deep Space Exploration. *Adv. Earth Sci.* 34 (10), 1001–1014.

Zhibao, D., Ping, L., and Chao, L. (2020). *Aeolian Geomorphology Map of Mars.* Xi'an: Xi'an Map Press.

Zurek, R. W., and Smrekar, S. E. (2007). An Overview of the Mars Reconnaissance Orbiter (MRO) Science mission. *J. Geophys. Res.* 112 (E5), E05S01. doi:10.1029/2006JE002701